Epineuston vortex recapture enhances thrust in tiny water skaters

Pankaj Rohilla[*a], **Johnathan N. O'Neil**[*a], **Chandan Bose**[b], **Victor M. Ortega-Jimenez**[c], **Daehyun Choi**[a], and **Saad Bhamla**[†a]

[a] *School of Chemical and Biomolecular Engineering, Georgia Institute of Technology, Atlanta, GA, USA*
[b] *Aerospace Engineering, School of Metallurgy and Materials, University of Birmingham, Birmingham, UK*
[c] *School of Biology and Ecology, University of Maine, ME, USA*

Vortex recapture underpins the exceptional mobility of nature's finest fliers and swimmers. Utilized by agile fruit flies and efficient jellyfish, this phenomenon is well-documented in bulk fluids. Despite extensive studies on the neuston—a vital fluidic interface where diverse life forms interact between air and water—neuston vortical hydrodynamics remain unexplored. We investigate epineuston (on water) vortical hydrodynamics in *Microvelia americana*, one of the smallest and fastest water striders, skating at 50 BL/s (15 cm/s). Their middle legs shed counter-rotating vortices, re-energized by hind legs, demonstrating epineuston vortex recapture. High-speed imaging, particle imaging velocimetry, physical models, and CFD simulations show re-energization increases thrust by creating positive pressure at the hind tarsi, acting as a virtual wall. This vortex capture is facilitated by the tripod gait, leg morphology, and precise spatio-temporal placement of the hind tarsi during the power stroke. Our study extends vortex recapture principles from bulk fluids to the neuston, offering insights into efficient epineuston locomotion, where surface tension and capillary waves challenge movement. Understanding epineuston vortex hydrodynamics can guide the development of energy-efficient microrobots to explore the planet's neuston niches, critical frontlines of climate change and pollution.

The unseen ballet of vortical forces orchestrates nature's most efficient swimmers and fliers [1–7]. These interactions, fundamental to minimizing energy expenditure and maximizing thrust, allow organisms to utilize energy from their own or others' wakes [1, 2, 8–10]. Jellyfish boost thrust by capturing vortices during relaxation, creating high-pressure zones [5, 11]. Fruit flies capture leading-edge vortices during the fling motion, minimizing the energy required to generate new vortices [12, 13]. Fish exhibit such efficient wake capture that even dead fish can swim upstream by resonating with oncoming Kármán street vortices [14, 15].

While these examples occur in bulk fluids, the neuston interface — a vital ecological niche — teems with life. From zooplankton, insects, and spiders to birds, reptiles, and plants, countless organisms interact at this boundary in marine and freshwater ecosystems [16–27]. Despite the challenges of balancing surface tension, drag, buoyancy, and capillary waves, no documented examples of vortex recapture at this interface exist. Driven by curiosity about neuston vortical interactions, we reveal a vortex re-energization mechanism in *Microvelia americana* (Hemiptera, Veliidae).

These millimeter-sized water walkers are epineustonic, living on the water surface and are one of the smallest and fastest on this ecological niche ($\mathbf{u}_B \sim 50$ BL/s, Figure 2.d). Part of the infraorder Gerromorpha, they are found in creeks and ponds worldwide and include over 200 species (Figure S1) [28–31]. Unlike most water striders that use elongated middle legs for rowing, *Microvelia* employ all six legs to walk and run using a tripod gait [16, 17, 32, 33]. Their unique morphology and kinematics enable them to recapture vortices shed from their middle legs, allowing them to speedily skate across the water surface. These amphibious insects, whose ancestors were terrestrial and used a tripod gait for movement on land, evolved to move on water while retaining this gait [16, 34–37]. Using high-speed imaging, particle imaging velocimetry, physical models, and CFD simulations, we describe the epineuston vortex interactions during the water skating behavior of *Microvelia*.

RESULTS

Skating on water. *Microvelia* possess dense hair coverage on their bodies and legs (Figure 1.a) [38]. SEM analysis reveals a tarsal hair density of $\sim 15,000$ hairs/mm^2 ($n = 3$), comparable to *Velia caprai* and *Gerridae*. [16, 39, 40]. This dense coverage enables *Microvelia* to maintain a Cassie-Baxter state [41], limiting water infiltration and maintaining superhydrophobicity leading to dimples at air-water surface contact points (Figure 1.b). The low Weber number, $We = \rho v^2 l/\sigma \ll 1$ (see Table S1) indicates that

*Equal contribution
†Corresponding author- ✉ saadb@chbe.gatech.edu

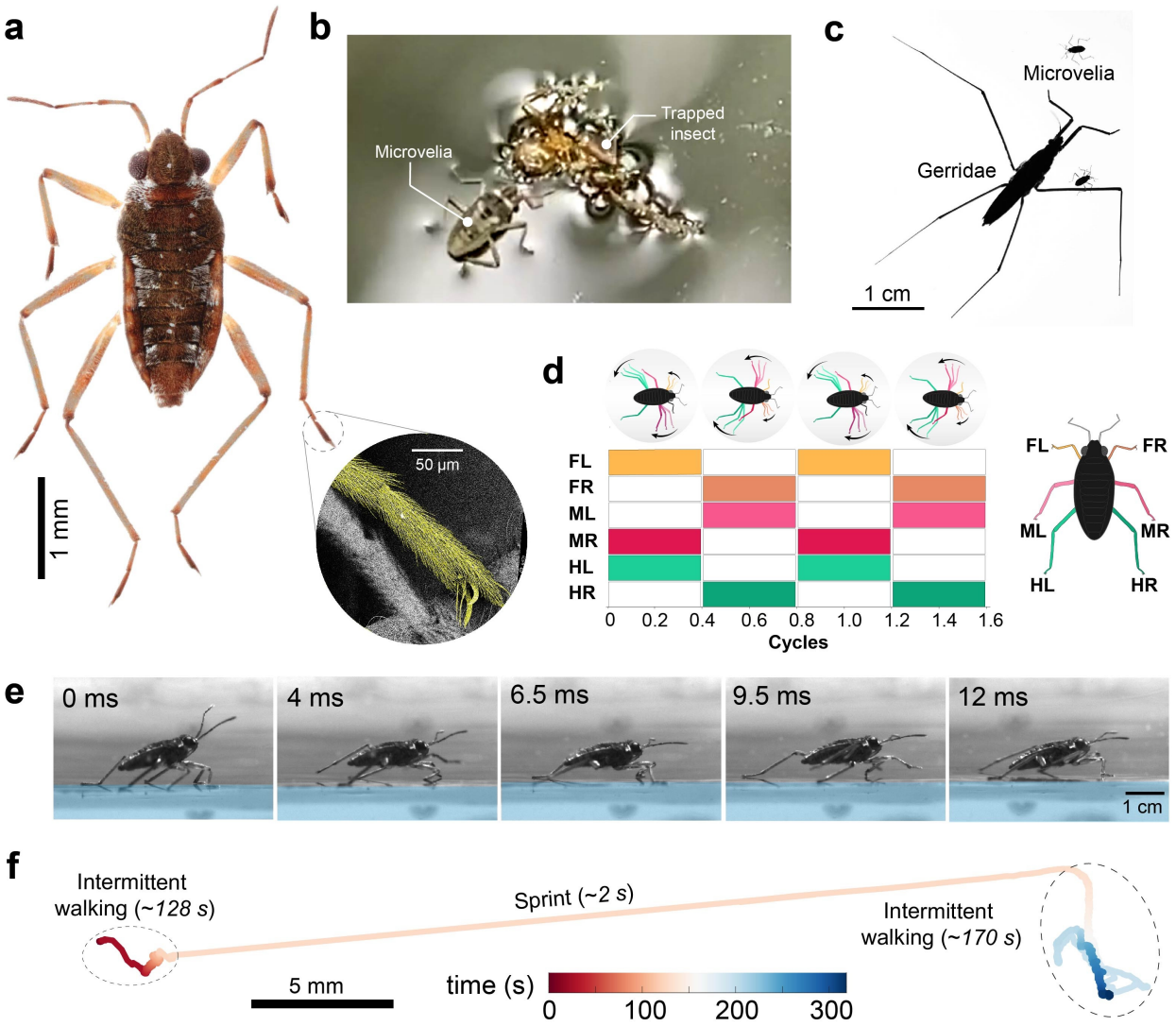

Figure 1: Behaviour and morphology of epineustonic *Microvelia americana* **(a)** Dorsal view of *Microvelia americana* with inset showing a SEM image of the dense hair coverage on middle leg tarsus (*pseudo-colored*). **(b)** *Microvelia Sp.* feeding on a trapped insect in a creek (Brunei), with legs deforming the water surface, forming dimples. **(c)** Size comparison showing *M. americana*'s small body size relative to commonly found water striders, *Gerridae*. **(d)** Alternating tripod gait plot for *M. americana* locomoting on water surface, showing the gait cycle of each leg performing power (color filled boxes) and recovery strokes (empty boxes). **(e)** Snapshots showing the side view of *M. americana* walking on water. **(f)** Dynamics of *M. americana* on water, indicating short skating escape-sprints (∼2 s) and intermittent walking behavior over a time span 5 minutes.

surface tension forces dominate over inertial forces in their interfacial locomotion, similar to other water striders like Gerridae [24].

Unlike water striders such as *Gerridae* that use a rowing gait, *Microvelia* employ an alternate tripod gait typical of terrestrial insects. In this gait, at least three legs – the front leg (FL), the contralateral middle leg (ML), and the ipsilateral hind leg (HL) – perform a power stroke on water (Figure 1.d,e), while the other legs recover in air or sometimes on water (SI Video 1).

To understand their epineustonic locomotion behavior, we examine their dynamics over a 5-minute period in the lab. During this time *Microvelia* primarily engage in intermittent walking, spending 99.6% of the time in this mode. However, they occasionally sprint as an escape response, skating a distance of ∼ 30 mm in ∼ 2 seconds (Figure 1.e). The temporal trajectory of the middle and hind legs shows overlapping paths during this skating mode, indicat-

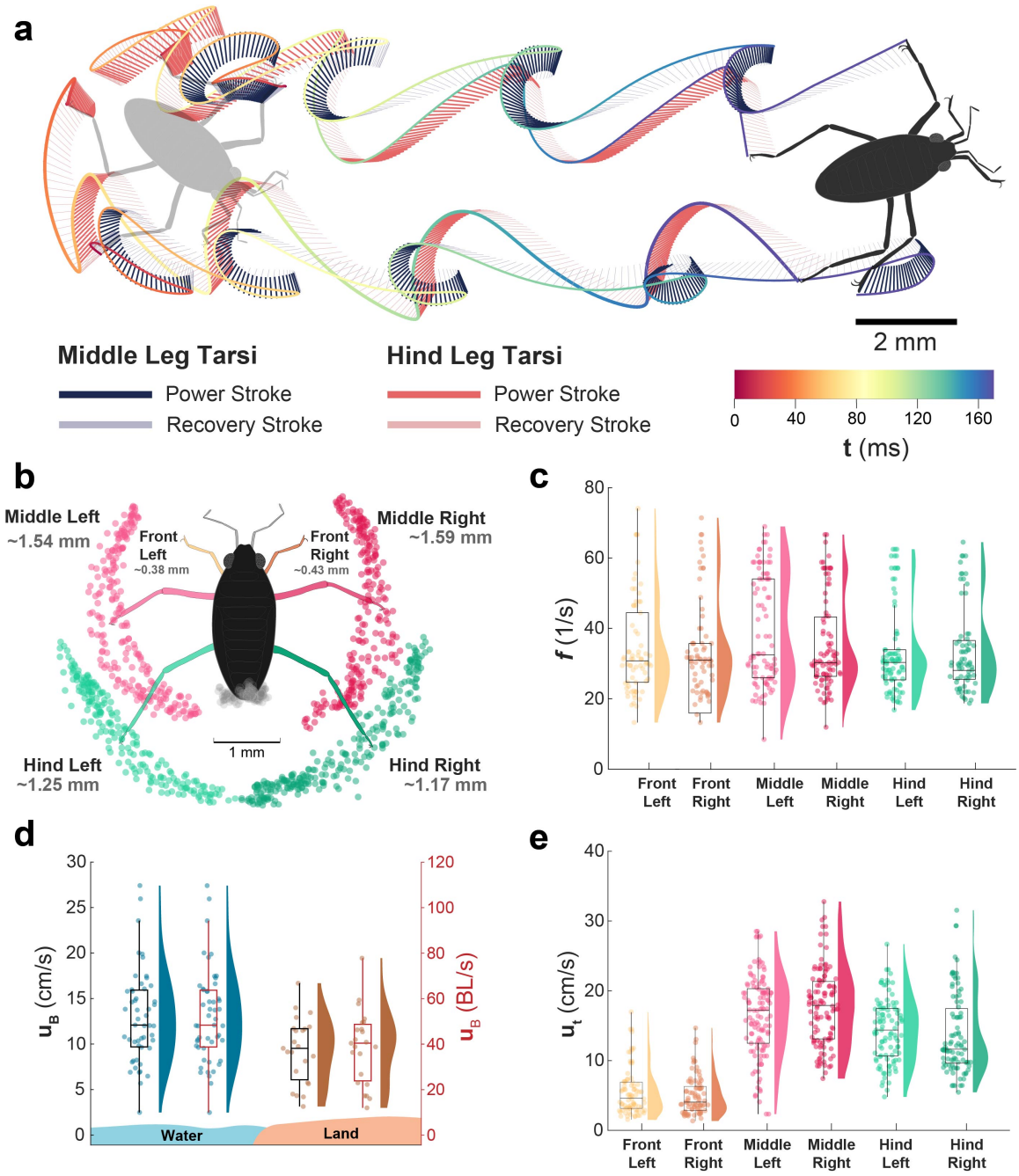

Figure 2: Epineustonic kinematics of *Microvelia*. **(a)** Tarsal trajectories of middle and hind legs of *Microvelia*. The solid lines represent the power strokes, while the faded blue and red lines show the recovery strokes. The trajectories illustrate the time spent by the tarsi during movement. **(b)** Stroke amplitudes of the middle and hind legs (n = 15), illustrated with their tarsal tip trajectories relative to the motion of their respective shoulder joints. The middle legs exhibit larger stroke amplitudes ($\lambda_{ML} \sim 1.54 \pm 0.43$ mm and $\lambda_{MR} \sim 1.59 \pm 0.74$ mm) compared to the hind legs ($\lambda_{HL} \sim 1.25 \pm 0.46$ mm and $\lambda_{HR} \sim 1.17 \pm 0.47$ mm). **(c)** Stroke frequency (N = 3, n = 15) of the middle and hind tarsi, showing an average stroke frequency of $f \sim 30$ strokes/s. **(d)** Body speed of *Microvelia* on water and land (styrofoam) in cm/s (left Y axis) and BL/s (body lengths per second, right Y axis). The average maximum body speed on water is ~ 15 cm/s (~ 50 BL/s), compared to ~ 10 cm/s (~ 40 BL/s) on land. **(e)** Peak tarsi speeds of *Microvelia* on water. The middle legs achieve higher peak linear speeds during power strokes (~ 17 cm/s) compared to the hind legs (~ 14 cm/s). This indicates that the middle legs act as the main hydrodynamic thrust propulsors, with higher acceleration (~ 2500 cm^2/s) compared to the hind legs (~ 2000 cm^2/s).

ing interfacial vortical interactions (Figure 2.a).

During the skating mode, the middle legs of *Microvelia* act as the main hydrodynamic thrust propulsors [32, 33]. These legs exhibit a stroke amplitude 23% larger than the hind legs, while maintaining the same stroke frequency (Figure 2.b,c). This larger amplitude allows for greater displacement with each stroke, enhancing thrust. The middle legs also achieve higher peak linear speeds during power strokes, 21% faster than the hind legs (Figure 2.e). This increased speed, coupled with greater acceleration—about 25% higher than that of the hind legs—indicates their dominant role as forceful thrust generators [33].

Epineuston hydrodynamic interactions. During the power stroke, the middle leg tarsi shed pairs of counter-rotating vortices (Figure 3.a, stage I). These vortices travel downstream, interacting with the hind tarsi, which enter the water at various spatio-temporal locations. The front tarsi generate weak vortices that dissipate without interacting with other tarsi (SI video II).

The exact location and timing of the incident hind tarsi relative to the vortices dictate the outcome of these interactions. Favourable interactions result in vortex re-energization, increasing the vortices' strength (Figure 3.a, Stage II and III). Body rocking and turning can misalign these interactions, altering the hind legs' angle of attack and leading to vortex annihilation or no interaction (Figure 3.b). Additionally, if *Microvelia* moves at high speed, its body can pass over the middle leg vortices before the hind legs can interact with them, emphasizing the importance of timing (Figure 3.f).

We measure the circulation of vortex pairs generated by the middle tarsi during re-energization until they dissipate after hind tarsi interaction. Circulation, $\Gamma = \int\int_s \omega.dS$, where ω is the vorticity and S is the bounded area, measures the vortices' strength. As the middle leg initiates the power stroke (Figure 3.c, point 1), the vortices' circulation increases, peaking at $\Gamma = 2$ cm^2/s (t = 71 ms), corresponding to the maximum tarsal speed (22 cm/s, t = 70 ms). The middle leg then decelerates, reducing Γ as the vortices dissipate (point 3). The hind tarsi then enters the wake, re-energizing the vortices to enhance the circulation to a second, lower peak of $\Gamma = 1.6$ cm^2/s (t = 88.5 ms) due to a lower hind-tarsal speed of 17 cm/s (Figure 3.c, point 4). This cycle ends with the hind tarsi completing their power stroke and dissipating the vortices (SI video II, Figure S2).

Across 52 instances in 6 specimens, we observe that 60% of the interactions result in re-energization, 27% show no interaction, and the remainder lead to vortex annihilation (Figure 3.e). We compare the normalized peak circulation before and after their hind tarsal interaction ($\tilde{\Gamma} = \Gamma_2/\Gamma_1$) with normalized body speed ($\tilde{\mathbf{u}} = \mathbf{u}_B/\mathbf{u}_t$) and the time interval (Δt) between strokes (Figure 3.d). Vortical re-energization primarily occurs when the hind tarsi strike between the middle tarsi vortices with shorter Δt (typically < 6 ms), during initial acceleration phase of the skating sprint (Figure 3.f). At higher body speeds, longer Δt, or due to body turning or rocking, the hind tarsi miss the vortices resulting in no interaction. When the hind legs skate across the pair of vortices rather than slaloming between them, the interactions tend to weaken the vortices, leading to vortex annihilation (Figure 3.d). Collectively, this reinforces that both the hind tarsi's entry position relative to the middle tarsi (angle-of-attack) and the inter-stroke interval play critical roles in determining the outcome of these interactions.

Epineuston vortical recapture increases thrust in *Microvelia*. Reconstructed pressure fields from PIV-measured velocity fields reveal insights into vortical interactions with the hind tarsi of *Microvelia* (Figure 4.a). During vortex re-energization, a local pressure gradient forms from upstream to downstream of the hind tarsi, generating the highest relative pressure ($\Delta p \sim 5$ Pa). In contrast, vortex annihilation results in lower relative pressure ($\Delta p \sim 2$ Pa, Figure S3), with cases of no interaction showing similarly low pressure.

We calculate the total impulse by integrating the relative pressure over time, $\mathbf{I} = \int_T \Delta p A dt$, where T is the duration of the power stroke and A is the planar area containing the tarsi and its wake (Figure S3). Normalizing the impulse, $\tilde{\mathbf{I}} = \int_T \Delta p dt/(\rho \bar{\mathbf{u}}_{t,n}^2 A)$, isolates the impact of hind tarsal interaction from tarsal speed. Excluding the impulse from the middle tarsi yields the relative impulse, $\tilde{\mathbf{I}}_r = \tilde{\mathbf{I}}/\tilde{\mathbf{I}}_{middle}$.

Our results show that vortex re-energization produces a normalized impulse ($\tilde{\mathbf{I}}_r \sim 1.08$), 34% higher than vortex annihilation (~ 0.81) and 15% higher than no interaction (~ 0.94) (Figure 4.b). This increased impulse results from enhanced fluid entrainment during re-energization, which raises pressure in the tarsal plane. When hind tarsi step into the center of the vortex pair, they entrain more fluid mass due to the converging flow driven by the vortical motion [44], leading to increased pressure and greater thrust.

The observed rise in normalized impulse during re-energization illustrates *Microvelia*'s ability to harness energy from its own wake, a phenomenon we call 'Epineuston Vortex Recapture'. Typically, wakes signifies lost energy to the environment. By step-

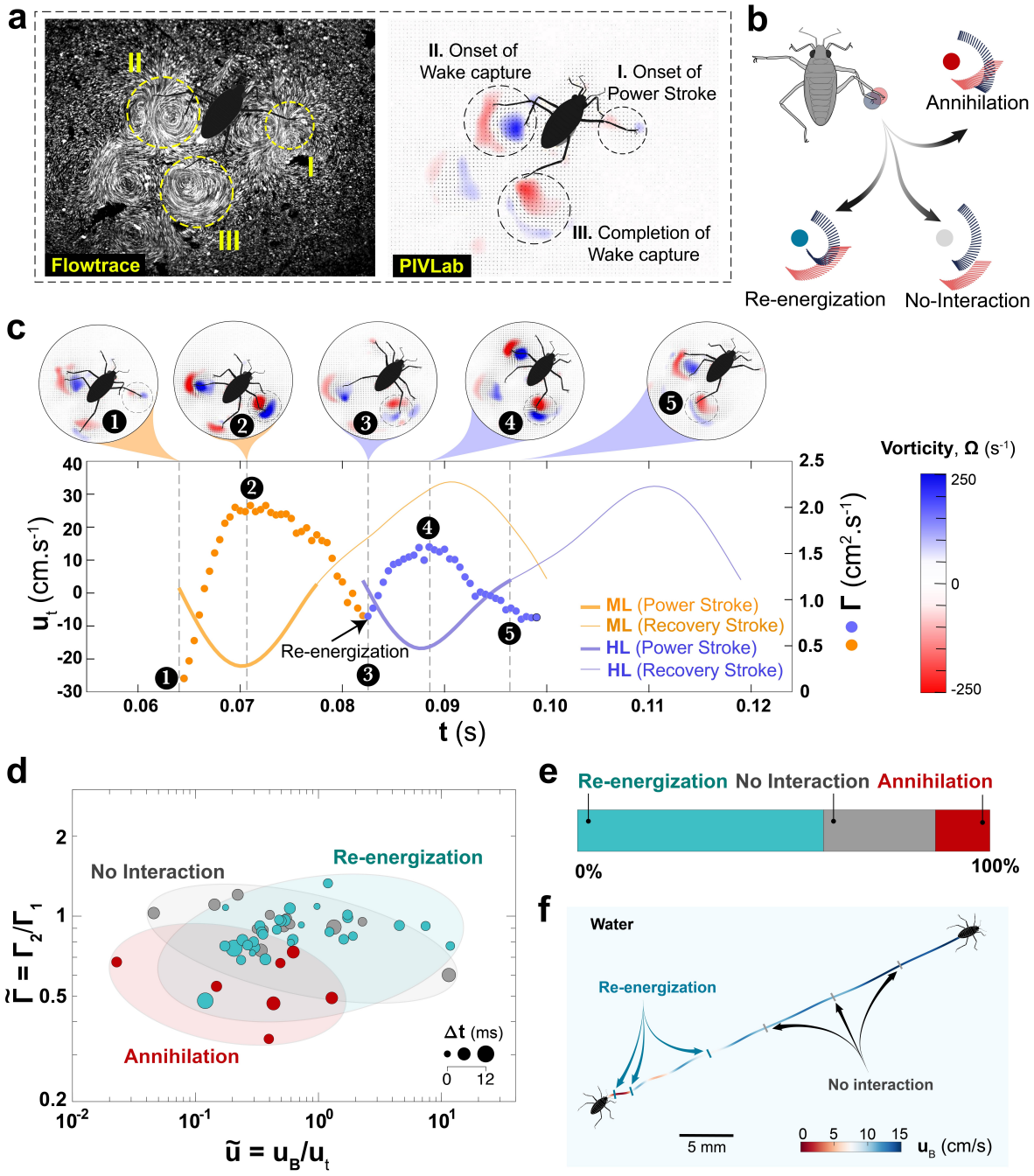

Figure 3: Hydrodynamic interactions in *Microvelia*'s epineustonic locomotion. **(a)** Stages of vortical shedding from the power strokes of the middle tarsus and their subsequent interactions with the hind tarsus. LHS: Flowfield streamlines visualization in Flowtrace [42] and RHS: vorticity field generated in PIVlab [43]. Stage I - Vortices generated during the onset of the power stroke of the middle right tarsus, (II) Hind legs stepping into the vortices shed from the middle left tarsus, (III) re-energized vortices from the hind right tarsus; LHS shows the vorticity field corresponding to the frame on the right. **(b)** Illustrations represent the three different outcomes of vortical interactions based on the trajectory of the hind and middle tarsi. **(c)** Representative tarsal velocity profiles of the middle-right and hind-right tarsi of *Microvelia* walking on water and the corresponding circulation (filled circles) of the vortices for the case of vortex re-energization. **(d)** Effect of normalized body speed (relative to hind tarsi speed) on the circulation ratio of vortices originating from the middle legs pre- and post-interactions with the hind tarsi. **(e)** Percentage outcomes of the vortical interactions of the hind tarsi with vortices shed from the middle tarsi, and **(f)** Different vortical interactions within a single run on water in *Microvelia*.

ping into vortices generated by its middle legs during previous strokes, *Microvelia* harnesses this energy to increase thrust production by the hind legs. This mechanism, driven by its tripod gait and interfacial movement, enables *Microvelia* to effectively generate thrust at the air-water interface.

Physical models validate inter-stroke interval in epineustonic vortical interactions. To evaluate the effect of inter-stroke intervals (Δt) on vortical interactions, we use a physical model. The model simulates *Microvelia*'s middle and hind tarsi power strokes on water, varying Δt to alter the hind tarsi's angle of attack to the vortices shed by the middle legs. The Reynolds number of the model ($\sim$18) is within the range of *Microvelia* ($Re \sim 2-21$, see Table S1). The first arm generates a counter-rotating vortex dipole, which the second arm interacts with, depending on Δt (Figure 4.c).

For large $\Delta t = -116$ ms, the first arm's vortices dissipate before the second arm's entry, resulting in no interaction (SI Video III, Figure S4). Reducing the interval allows for re-energization, with the second arm's vortices showing higher normalized circulation ($\tilde{\Gamma} > 1$) (Figure 4.d). However, at very short intervals ($-10 < \Delta t < 10$ ms), capillary waves generated by the arms disrupt the vortices, leading to annihilation. The normalized circulation ($\tilde{\Gamma}$) compares both *Microvelia* and the physical model, revealing that optimal inter-stroke intervals enhance re-energization and thrust (Figures S4, S5). Vortical re-energization in *Microvelia* doesn't always imply $\tilde{\Gamma} > 1$ due to reduced hind legs' tarsal speed, imparting less energy to the vortices (Figure 2.e).

CFD analysis of thrust enhancement during vortex re-energization. We simulate thrust enhancement through vortex capture using 2D CFD models of high aspect ratio ($AR = 20$) rectangular plates undergoing prescribed rotation and translation. Mimicking the physical model configuration, the first plate rotates counterclockwise, and the second rotates clockwise, starting with a time gap (Δt), traversing the first plate's vortical wake (SI Video 4, Figure S5). These simulations evaluate the role of vortex re-energization on thrust via robotic arms' trajectory rather than mimicking the precise kinematics of *Microvelia*.

Streamline analysis shows differences in flow velocity magnitudes for different Δt intervals (Figure 4.e). For $\Delta t = 0.2$ s, the second plate captures the first plate's wake, entering its recirculation region closely (SI video 4). As a result, the vortex cores with the same sense of rotation from both plates co-align to increase the resultant circulation, augmenting the propulsive force. In contrast, for $\Delta t = 0.5$ s, the second plate fails to interact effectively, leading to vortex annihilation with lower flow velocities and thrust due to the absence of effective wake capture.

To reinforce our findings, we present the temporal evolution of the coefficient of thrust (C_T) for the second plate, showing vortical re-energization, compared to no interaction (Figure 4.f). The C_T, defined as $2T/(\rho_f \mathbf{u_r}^2 A)$, where T is the thrust force, ρ_f is the fluid density, $\mathbf{u_r}$ is the relative linear velocity, and A is the plate's projected area, illustrates the influence of interaction on vorticity fields at different times.

For $\Delta t = 0.2$ s, C_T peaks at $t = 1.2$ s as vortex dipoles from both plates interact, augmenting circulation. As the plates separate, C_T decreases, showing reduced wake interaction. Thrust enhancement via wake capture correlates with changes in fluid impulse, influenced by circulation and vortex core velocities. This unsteady flow situation is consistent with pressure data from *Microvelia* and the physical model (Figure 4.a,b), where optimal stroke timing increases entrainment and thrust, demonstrating enhanced thrust through vortex re-energization.

Conclusions and Outlook

Our findings illuminate vortical interactions within the neuston, the dynamic water-air boundary that supports diverse life forms. *Microvelia*, among one of the smallest and fastest epineustonic animals, create nearly 2D vortices due to their minute size and weight, forming shallow dimples on the water surface [45, 46]. Their alternating tripod gait, inherited from terrestrial ancestors, enables versatile movement across water, land, and duckweed [17, 32, 47].

Although less energy-efficient than rowing gait, the alternatig tripod gait excels in amphibious locomotion, providing *Microvelia* with a strategic advantage in foraging and evading predators [16, 24, 46]. This gait and leg proportions faciliate epineustron vortex recapture combination, where hind leg tarsi boost the circulation and fluid entrainment of vortices shed by middle legs. This re-energization creates a positive pressure at the hind tarsi, acting as a virtual wall that augments thrust [46]. In other genera such as *Mesovelia*, longer middle legs prevent effective vortex recapture, underscoring the critical role of leg size in this mechanism (Figure S7).

Epineuston vortex interactions hinge on the spatial location, angle of attack, and trajectory of hind leg tarsi, determining whether vortices are re-energized, annihilated, or minimally interacted with. Our robotic arm physical model and CFD simulations reinforce the impact of inter-stroke intervals on these interactions. The data indicate that optimal timing

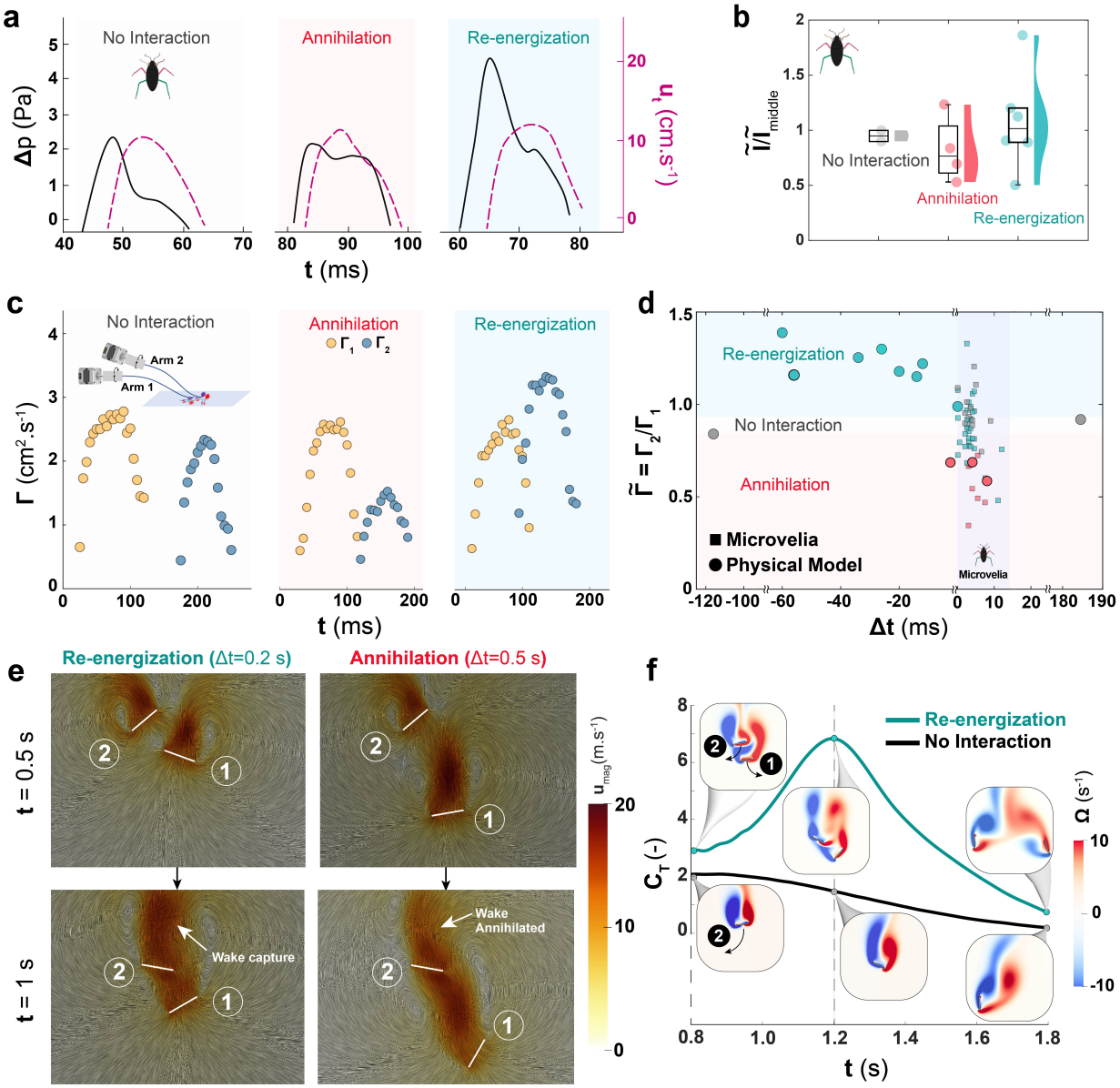

Figure 4: Quantifying epineuston vortical interactions through physical models and CFD analysis. (a) Temporal evolution of relative pressure ($\mathbf{\Delta P}$) and tarsal speed ($\mathbf{v}_t$) of the hind leg. No-interaction and annihilation cases represent the the hind left tarsi, while re-energization corresponds to the hind right tarsi. **(b)** Normalized impulse for different types of vortical interaction. The semi-violin plot shows the distribution of the data as a jitter plot, while the box and whisker plot represent the median and the four quartiles (25%, 50%, 75%, and 100%) for *Microvelia* specimens (N=3) and strokes ($n = 12$). **(c)** Temporal evolution of the vortex circulation $\mathbf{\Gamma}$ for each robotic arm with varying Δt showing different vortical interaction outcomes. **(d)** Regime map of normalized circulation ($\mathbf{\Gamma_2/\Gamma_1}$) for varying Δt. $\mathbf{\Gamma_1}$ and $\mathbf{\Gamma_2}$ represent peak circulation from the middle leg (or first arm) and hind leg (or second arm), respectively (N=7, n=53). **(e)** CFD results showing effect of the time interval between plate movements (in quiescent fluid) on vortical interactions depicted by velocity magnitude contours. The second plate starts moving at $t = 0$ s with $\Delta t = 0.2$ s for re-energization and $\Delta t = 0.5$ s for annihilation. In snapshots at $t = 1$ s, arrows indicates the enhanced and reduced velocity field due to wake capture and wake annihilation respectively. **(f)** Temporal evolution of the coefficient of thrust (C_T) of the second plate for re-energization and no interaction. Snapshots show the interaction's impact on instantaneous vorticity fields at different times.

and positioning of leg strokes enhance thrust through vortex re-energization, offering new insights into fluid dynamics at the air-water interface. Exploring microvelia juvenile nymphs, multiphase CFD simulations, and turbulent flow regimes will further deepen our understanding of these interactions.

By uncovering the physics behind the vortical recapture in *Microvelia*, we extend similar mechanisms observed in jellyfish and fruit flies to the neuston [5, 11, 12]. Epineuston vortex recapture could inspire the development of efficient water-skating devices and amphibious robots, enhancing our exploration of the oceanic and freshwater neuston niches [26].

ACKNOWLEDGMENTS

The authors thank the members of the Bhamla Lab for their feedback and useful discussions. MSB acknowledges funding support from the NSF Grants CAREER 1941933 and PHY-2310691, and gift funding from the Open Philanthropy Project. PR acknowledges the funding support from the Eckert Postdoctoral Fellowship, Georgia Tech. J.O. acknowledges funding support from the GT UCEM fellowshp program and the Herbert P. Haley fellowship program.

COMPETING INTERESTS

The authors declare no competing interests.

REFERENCES

[1] John O Dabiri. Optimal vortex formation as a unifying principle in biological propulsion. *Annual review of fluid mechanics*, 41:17–33, 2009.

[2] PF Linden and JS Turner. 'Optimal' vortex rings and aquatic propulsion mechanisms. *Proceedings of the Royal Society of London. Series B: Biological Sciences*, 271(1539):647–653, 2004.

[3] Erik J Anderson and M Edwin DeMont. The mechanics of locomotion in the squid loligo pealei: locomotory function and unsteady hydrodynamics of the jet and intramantle pressure. *Journal of Experimental Biology*, 203(18):2851–2863, 2000.

[4] Michael S Triantafyllou, GS Triantafyllou, and DKP Yue. Hydrodynamics of fishlike swimming. *Annual review of fluid mechanics*, 32(1):33–53, 2000.

[5] John H Costello, Sean P Colin, John O Dabiri, Brad J Gemmell, Kelsey N Lucas, and Kelly R Sutherland. The hydrodynamics of jellyfish swimming. *Annual Review of Marine Science*, 13:375–396, 2021.

[6] Iztok Lebar Bajec and Frank H Heppner. Organized flight in birds. *Animal Behaviour*, 78(4):777–789, 2009.

[7] John Roger Speakman and D Banks. The function of flight formations in greylag geese anser anser; energy saving or orientation? *International Journal of Avian Science*, 140(2):280–287, 1998.

[8] Hao Liu, Shizhao Wang, and Tianshu Liu. Vortices and forces in biological flight: Insects, birds, and bats. *Annual Review of Fluid Mechanics*, 56:147–170, 2024.

[9] You-Jun Lin, Sheng-Kai Chang, Yu-Hsiang Lai, and Jing-Tang Yang. Beneficial wake-capture effect for forward propulsion with a restrained wing-pitch motion of a butterfly. *Royal Society open science*, 8(8):202172, 2021.

[10] Nils B Tack, Kevin T Du Clos, and Brad J Gemmell. Fish can use coordinated fin motions to recapture their own vortex wake energy. *Royal Society Open Science*, 11(1):231265, 2024.

[11] Brad J Gemmell, Sean P Colin, and John H Costello. Widespread utilization of passive energy recapture in swimming medusae. *Journal of Experimental Biology*, 221(1):jeb168575, 2018.

[12] Fritz-Olaf Lehmann, Hao Wang, and Thomas Engels. Vortex trapping recaptures energy in flying fruit flies. *Scientific Reports*, 11(1):6992, 2021.

[13] Michael H Dickinson, Fritz-Olaf Lehmann, and Sanjay P Sane. Wing rotation and the aerodynamic basis of insect flight. *Science*, 284(5422):1954–1960, 1999.

[14] David N Beal, Franz S Hover, Michael S Triantafyllou, James C Liao, and George V Lauder. Passive propulsion in vortex wakes. *Journal of fluid mechanics*, 549:385–402, 2006.

[15] Liang Li, Máté Nagy, Jacob M Graving, Joseph Bak-Coleman, Guangming Xie, and Iain D Couzin. Vortex phase matching as a strategy for schooling in robots and in fish. *Nature communications*, 11(1):5408, 2020.

[16] N Møller Andersen. A comparative study of locomotion on the water surface in semiaquatic bugs

(insecta, hemiptera, gerromorpha). *Vidensk. Meddel. Natuirist. Foren. Kjobenhavn*, 139:337–396, 2016.

[17] Antonin JJ Crumiere, M Emilia Santos, Marie Sémon, David Armisén, Felipe FF Moreira, and Abderrahman Khila. Diversity in morphology and locomotory behavior is associated with niche expansion in the semi-aquatic bugs. *Current Biology*, 26(24):3336–3342, 2016.

[18] Jeffrey W. Shultz. Walking and Surface Film Locomotion in Terrestrial and Semi-Aquatic Spiders. *Journal of Experimental Biology*, 128(1):427–444, 03 1987.

[19] S Tonia Hsieh and George V Lauder. Running on water: Three-dimensional force generation by basilisk lizards. *Proceedings of the National Academy of Sciences*, 101(48):16784–16788, 2004.

[20] Glenna T Clifton, Tyson L Hedrick, and Andrew A Biewener. Western and clark's grebes use novel strategies for running on water. *The Journal of Experimental Biology*, 218(8):1235–1243, 2015.

[21] Victor M Ortega-Jimenez, Elio J Challita, Baekgyeom Kim, Hungtang Ko, Minseok Gwon, Je-Sung Koh, and M Saad Bhamla. Directional takeoff, aerial righting, and adhesion landing of semiaquatic springtails. *Proceedings of the National Academy of Sciences*, 119(46):e2211283119, 2022.

[22] S Wang and AM Ardekani. Swimming of a model ciliate near an air-liquid interface. *Physical Review E*, 87(6):063010, 2013.

[23] Jonathan Voise and Jérôme Casas. The management of fluid and wave resistances by whirligig beetles. *Journal of The Royal Society Interface*, 7(43):343–352, 2010.

[24] David L Hu and John WM Bush. The hydrodynamics of water-walking arthropods. *Journal of Fluid Mechanics*, 644:5–33, 2010.

[25] Zexiang Huang, Hao Yang, Ke Xu, Jianing Wu, and Jinxiu Zhang. Collecting differently sized particles on water surface by maneuvering pedal waves on the foot of the water snail pomacea canaliculata. *Soft Matter*, 18(40):7850–7858, 2022.

[26] Rebecca R Helm. The mysterious ecosystem at the ocean's surface. *PLoS Biology*, 19(4):e3001046, 2021.

[27] Lanna Cheng and Himanshu Mishra. Why did only one genus of insects, halobates, take to the high seas? *PLoS Biology*, 20(4):e3001570, 2022.

[28] Aidamalia Vargas-Lowman, David Armisen, Carla Fernanda Burguez Floriano, Isabelle da Rocha Silva Cordeiro, Séverine Viala, Mathilde Bouchet, Marie Bernard, Augustin Le Bouquin, M Emilia Santos, Alexandra Berlioz-Barbier, et al. Cooption of the pteridine biosynthesis pathway underlies the diversification of embryonic colors in water striders. *Proceedings of the National Academy of Sciences*, 116(38):19046–19054, 2019.

[29] Matthew R Pintar, Jeffrey L Kline, and Joel C Trexler. The aquatic heteroptera (hemiptera) of marshes in the florida everglades. *Florida Entomologist*, 104(4):307–319, 2021.

[30] JT Polhemus. Water-striders (hemiptera: Gerridae, veliidae, etc.). *Marine insects. Elsevier, Amsterdam*, pages 187–224, 1976.

[31] Nils Møller Andersen. Microvelia polhemi, n. sp. (heteroptera: Veliidae) from dominican amber: The first fossil record of a phytotelmic water strider. *Journal of the New York Entomological Society*, 107:135–144, 1999.

[32] Johnathan Nathaniel O'Neil, Kai Lauren Yung, Gaetano Difini, Holden Walker, and M Saad Bhamla. Tiny amphibious insects use tripod gait for seamless transition across land, water, and duckweed. *bioRxiv*, pages 2024–04, 2024.

[33] Johnathan Nathaniel O'Neil, Kai Lauren Yung, Gaetano Difini, Pankaj Rohilla, and M Saad Bhamla. Limb loss and specialized leg dynamics in tiny water-walking insects. *bioRxiv*, pages 2024–04, 2024.

[34] Nils Møller Andersen. Phylogenetic inference as applied to the study of evolutionary diversification of semiaquatic bugs (hemiptera: Gerromorpha). *Systematic Zoology*, 28(4):554–578, 1979.

[35] Miguel Piñeirua, Anna Verbe, and Jérôme Casas. Substrate-mediated leg interactions play a key role in insect stability on granular slopes. *Physical Review E*, 108(1):014903, 2023.

[36] Antoine Humeau, Miguel Piñeirua, Jérôme Crassous, and Jérôme Casas. Locomotion of ants walking up slippery slopes of granular materials. *Integrative Organismal Biology*, 1(1):obz020, 2019.

[37] Pavan Ramdya, Robin Thandiackal, Raphael Cherney, Thibault Asselborn, Richard Benton, Auke Jan Ijspeert, and Dario Floreano. Climbing favours the tripod gait over alternative faster insect gaits. *Nature communications*, 8(1):14494, 2017.

[38] Lanna Cheng. Marine and freshwater skaters: differences in surface fine structures. *Nature*, 242(5393):132–133, 1973.

[39] Nils Møller Andersen. Fine structure of the body hair layers and morphology of the spiracles of semiaquatic bugs (insecta, hemiptera, gerromorpha) in relation to life on the water surface. *Vidensk. Medd. Dansk Naturhist. Foren.*, 140:7–37, 1977.

[40] Cédric Finet, Amélie Decaras, Maria Rutkowska, Pascale Roux, Samuel Collaudin, Pauline Joncour, Séverine Viala, and Abderrahman Khila. Leg length and bristle density, both necessary for water surface locomotion, are genetically correlated in water striders. *Proceedings of the National Academy of Sciences*, 119(9):e2119210119, 2022.

[41] ABD Cassie and S Baxter. Wettability of porous surfaces. *Transactions of the Faraday society*, 40:546–551, 1944.

[42] William Gilpin, Vivek N Prakash, and Manu Prakash. Flowtrace: simple visualization of coherent structures in biological fluid flows. *Journal of experimental biology*, 220(19):3411–3418, 2017.

[43] William Thielicke and René Sonntag. Particle image velocimetry for matlab: Accuracy and enhanced algorithms in pivlab. *Journal of Open Research Software*, 9(1), 2021.

[44] Michael Krieg and Kamran Mohseni. Modelling circulation, impulse and kinetic energy of starting jets with non-zero radial velocity. *Journal of Fluid Mechanics*, 719:488–526, 2013.

[45] Robert B Suter. Spider locomotion on the water surface: biomechanics and diversity. *The Journal of Arachnology*, 41(2):93–101, 2013.

[46] Thomas Steinmann, Antoine Cribellier, and Jérôme Casas. Singularity of the water strider propulsion mechanisms. *Journal of Fluid Mechanics*, 915, 2021.

[47] Stephen P Yanoviak and DN Frederick. Water surface locomotion in tropical canopy ants. *Journal of Experimental Biology*, 217(12):2163–2170, 2014.